Growth of the Tian Shan drives migration of the conglomerate-sandstone transition in the southern Junggar foreland basin

Migration of the conglomerate-sandstone transitions in the southern Junggar foreland basin driven by the growth of northern Tian Shan through time

Chao Li[ab], ShengLi Wang[b*], Yongxiang Li[b], Yan Chen[c], Hugh Sinclair[d], Dongtao Wei[e], Delong Ma[f], Huayu Lu[g], Xianyan Wang[g], Liangshu Wang[b]

a School of Earth Sciences and Engineering, Hohai University, Nanjing 211100, China;

b School of Earth Sciences and Engineering, Nanjing University, Nanjing 210023, China;

c Institut des Sciences de la Terre d'Orléans; Bâtiment Géosciences, rue de Saint Amand, BP 6759, 45067 Orléans Cedex 2, France;

d School of GeoSciences, University of Edinburgh, Edinburgh EH8 9XP, UK;

e Xi'an Center of China Geological Survey, Xi'an 710054, China;

f Research Institute of Petroleum Exploration and Development—Northwest, PetroChina, Lanzhou 730020, China;

g School of Geography and Ocean Science, Nanjing University, Nanjing 210023, China

ABSTRACT:

The conglomerate-sandstone transition in a foreland basin-fill is controlled by tectonics and climate, and can act as an alternative shortening indicator in the orogen-foreland basin system. Two seismic profiles across northern Tian Shan foreland basin image the Cenozoic sedimentary succession, providing an opportunity to quantify the evolution of the transition in the foreland basin with the growth of the orogenic belt. We identified the horizontal position of the transitions along each seismic reflector among the basin-fill relative to the basin basement according to the seismic character of these two seismic profiles, on basis of distinct seismic phases of these two types of deposits. The ages of these reflectors are determined by correlating them with magnetostratigraphic sections. The linear regression model between positions and ages of the transitions indicate that the transitions migrated northward at a rate of ~0.36 mm/yr along 84°E during 23–6 Ma, and at ~4.03 mm/yr along 87°E during 3.1–0.7 Ma. The migration rates contain the lateral propagation of northern Tian Shan and the crustal shortening. The deviations between the observed and predicted positions of the transition demonstrate six cycles of climate oscillations during 23–6 Ma, and four cycles during 3.1–0.7 Ma in northern Tian Shan. The average cycle

since the Pliocene became shorter, consistent with a change from a stable climate to one with frequent, high-amplitude variations occurring since the Quaternary based on the Oxygen stable isotope record.

KEYWORDS: conglomerate-sandstone transition, southern Junggar foreland basin, northern Tian Shan, shortening, seismic profiling

INTRODUCTION

Sediment from active mountain ranges fines downstream due to size-selective sorting and abrasion into sediment routing systems, and accumulates in sedimentary basins ultimately (e.g., Paola et al., 1992; Allen and Heller, 2012). The transition in sediment grain sizes, from gravel to sand over a short downstream distance, is termed the gravel-sand transition (GST) (Ferguson et al., 1996). The GST is archived in a sedimentary basin as a conglomerate-sandstone transition (e.g., Dubille and Lavé, 2015). Positions of conglomerate-sandstone transitions in a foreland basin succession are determined by basin subsidence rates, sediment supplies and geomorphic conditions, and all these factors depend on tectonic or climatic forcings in the adjacent orogen (Dingle et al., 2017). Hence, the conglomerate-sandstone transitions in a foreland basin are moving boundaries that migrate in response to the shortening forcing in the foreland basin-orogen system as well the climatic one (e.g., Burbank et al., 1988; Rohais et al., 2012; Schlunegger and Norton, 2015; Dingle et al., 2016). For example, the progressive forelandward migration of the conglomerate-sandstone transitions through time driven by the orogeny was observed in the Ganga foreland basin (Dubille and Lavé, 2015) and the foreland basins to both sides of Tian Shan (Charreau et al., 2009a). Hence, quantifying of spatial-temporal evolution of the transitions provides an alternative method to constrain shortening in a foreland basin-orogen system, besides thrusting and folding (e.g., Avouac et al., 1993; Qiu et al., 2019), and migration of the coupled foreland basins (e.g., Naylor and Sinclair, 2008; Wang et al., 2021). The key to implementing the method is constraining the accurate positions and ages of transitions in the foreland basin-fill.

The late Cenozoic strata in foreland basins to both sides of Tian Shan (Fig. 1) are characterized by radical grain size transitions from sandstone to conglomerate in upwards coarsening fluvial successions (Zhou et al., 1988; Zhang et al., 2001). The transition is interpreted as a diachronous facies transition resulted from the propagation of the thrust wedge and the crustal shortening (Charreau et al., 2009a). For nearly two decades, voluminous high-quality seismic profiles and well

data have been acquired for hydrocarbon exploration in southern Junggar foreland basin (Fig. 1b) where ages of the Cenozoic strata have been well constrained by magnetostratigraphic studies (e.g., Charreau et al., 2009b，Lu et al., 2010). These works provide bases for deciphering the filling process of the foreland basin with the growth of Tian Shan, and understanding the roles of tectonics and climatic change in this process. Here, we present two northeast-trending seismic profiles across southern Junggar foreland basin (Figs. 1 and 2). They show that almost each seismic reflector in the late Cenozoic strata has a seismic phase transition, which corresponds to the conglomerate-sandstone transition in the basin-fill based on well logging data and field observations. We correlated the seismic reflectors to the nearest magnetostratigraphic ages (Charreau et al., 2009b，Lu et al., 2010). A linear regression model of positions and ages of the transitions demonstrates its northward migration rate representing the propagation of northern Tian Shan and the crustal shortening. The observed deviations from the model could represent the climatic oscillations in the northern Tian Shan area.

GEOLOGICAL SETTING

The Indian-Asian Collision caused the rejuvenation of Paleozoic Tian Shan in central Asia (Windley et al., 1990; Avouac et al., 1993) to form a Cenozoic intracontinental orogen (Fig. 1). Building up of the range induced flexural subsidence of the foreland basins to its both sides. The southern Junggar foreland basin north of the range contains an ~5,000 m thick Cenozoic succession, which is divided into the Ziniquanzi, Anjihaihe, Shawan, Taxihe, Dushanzi and Xiyu Formations in an ascending order (BGMRX, 1993), the upper four formations of which thin northwards (Wang et al., 2013). Sedimentary environments in the basin changed from lacustrine in the Oligocene to fluvial-alluvial fan since the late Miocene (BGMRX, 1993; Charreau et al., 2009a). Well data reveal continental fluvial plain and intermittent diluvial fan during deposition of the Dushanzi Formation, flood plain and fluvial fan during deposition of the Xiyu Formation (Fig. S4).

SEISMIC DATA

The AA' seismic reflection profile, 23-km-long and 4-second-deep (Fig. 2a), crosses the western part of the southern Junggar foreland basin (Fig. 1); the BB' profile, 30-km-long and 4-second-deep (Fig. 2b), crosses the eastern part of the basin. They show that each reflector above the base of the Anjihaihe Formation has two style of seismic phases: high amplitude, semi-continuous, and hummocky to the south, and high amplitude and continuous to the north(Fig. 2a and b),

which are generally interpreted as different lithologies (He et al., 2005). The former represents the alluvial gravel deposits in front of the range; and the latter stands for finer-grained deposits mainly composed of sandstone. Well data and our field observations of modern fluvial sediment (Fig. 1) testified that the seismic phase transition of each reflector corresponds to the conglomerate-sandstone transition of a deposit layer in the basin-fill, which is consistent with the interpretation of the identical seismic phase transition in the southern Tian Shan foreland basin (He et al., 2005; Charreau et al., 2009a).

LOCATING CONGLOMERTE-SANDSTONE TRANSITONS

We tracked all the seismic reflectors in the profiles for locating the horizontal position of the seismic phase transition of each reflector, which represents the position of the conglomerate-sandstone in each layer of the basin-fill. The lowest seismic phase transitions in profiles AA' and BB' are used as referencing lines for locating the transition.

We recognized 44 seismic reflectors in profile AA', named R1 through R44 in an ascending order (Figs. 2a and S1; Table S1). Reflectors R1–R10, R11–R17 and R18–R45 occur in the Shawan, Taxihe and Dushanzi Formations, respectively (Fig. 2a). From R2, the bottom of the Shawan Formation to R43, the top of the Dushanzi Formation, the seismic phase transitions migrate ~7.64 km northward, but it backstepped to the south six times. Considering the angle between the direction of profile AA’ and the trend of Tian Shan is ~62°, we projected displacements of the conglomerate-sandstone transitions in the direction perpendicular to Tian Shan (Table S1; Fig. 3a) to retrieve migration of the transitions relative to the range. The impedance difference between rocks to the south and north sides of the transitions from the upper Dushanzi Formation to the lower Xiyu Formation decreases to a level that cannot be detected (Fig. 2a). Four continuous parallel reflectors in the most-upper Xiyu Formation extend to the southern boundary of the profile, which may correspond to Quaternary eolian beds in the northern front of Tian Shan (Fig. S4; Fang et al., 2002).

In profile BB', we tracked 37 sub-parallel reflectors from the lower Dushanzi Formation to the middle Xiyu Formation, named H1 through H37 in an ascending order (Figs. 2b and S5). The seismic phase transition occurs from H17 to H33 in the middle Dushanzi Formation through the lower Xiyu Formation (Table S2). The transitions migrate ~12.32 km northward. The upper Xiyu Formation is not imaged completely in the seismic profile. We also projected displacements of the

transition in profile BB' to the direction perpendicular to Tian Shan (Table S2; Fig. 3b), due to the angle of ~54° between the direction of the profile and the trend of Tian Shan.

AGE CONTROL OF SEISMIC REFLECTORS

Magnetostratigraphic studies (Charreau et al., 2009a; 2009b) reveal that the bottom ages of the Xiyu and Dushanzi Formations along northern Tian Shan are significantly diachronous. Therefore, we assigned ages of the late Cenozoic strata in profile AA' or BB' (Fig. 2) by correlating them with the nearest magnetostratigraphic sections, respectively. Assuming a constant sedimentation rate representing any two consecutive reflectors, ages of all seismic reflectors in the Shawan Formation through the Xiyu Formations were interpolated (Table S1 and Table S2).

MIGRATION OF CONGLOMERATE-SANDSTONE TRANSITIONS

We quantified the relationship between the positions (y) and ages (x) of the transitions by establishing their linear regression model (Fig. 3a and b). For profile AA', the regression equation is $y = 9.112 - 0.358x$, $R^2 = 0.98$, demonstrating that the conglomerate-sandstone migrated ~6.75 km northward at a rate of ~0.36 mm/yr during 23–6 Ma (V_{mc} in Fig. 3d). We calculated the deviations between the observed and predicted positions of the transitions in the model. The positive deviations indicate that the observed positions are located on the north side of the predicted ones, and the negative value means the opposite (Fig. 3). There are six cycles of the deviation values of the transitions in profile AA' during 23–6 Ma (Fig. 4), with an average cycle of ~3.0 Myr.

For profile BB', the regression equation is $y = 12.804 - 4.121x$, $R^2 = 0.98$ (Fig. 3b), revealing that the transitions migrated ~10.0 km northward at a rate of ~4.03 mm/yr during 3.1–0.7 Ma (V_{mc} in Fig. 3d). There are four cycles of the deviation between the observed and predicted positions of the transitions during 3.1–0.7 Ma (Fig. 4), with an average cycle of ~0.5 Myr.

DISCUSSION

These two seismic profiles across the southern Junggar foreland basin show that seismic reflectors among late Cenozoic strata are characterized by the seismic phase transition along each reflector, which demonstrates a significant impedance contrast between rocks to the north and south of the transition, resulting from different lithologies. Our field observations

and well data in the active basin indicate that the seismic phase transition of a seismic reflector corresponds to the conglomerate-sandstone of a sedimentary layer (He et al., 2005; Charreau et al., 2009b). Profiles AA' and BB' reveal that the transitions in the basin migrated northward at a million-year scale, but oscillated several times in the north-south trend in a short term (Figs. 3 and 4). The linear regression between the positions and ages of the transitions recognized from these profiles indicates that the GST migrated at a constant rate of ~0.36 mm/yr along 84°E during 23–6 Ma and ~4.03 mm/yr along 87°E during 3.1–0.7 Ma. The deviations between the observed and predicted positions of the transitions show six cycles during 23–6 Ma and four cycles during 3.1–0.7 Ma.

Research on downstream grain size fining trends in sedimentary basins reveals that the position of a GST is controlled by basin subsidence rates, sediment supplies and geomorphic conditions (Paola et al., 1992; Dingle et al., 2017). These factors in an orogen-foreland basin system are mainly determined by orogenesis (Davis et al., 1983; DeCelles and Giles, 1996). The horizontal displacement of the orogenic wedge relative to the basin basement drives the forelandward progressive progradation of the GST (DeCelles and DeCelles, 2001; Naylor and Sinclair, 2008), which is archived as conglomerate-sandstone in the basin. This indicates the migration rate of the conglomerate-sandstone transitions through time is the same with the foreland basin at a million-year-time scale ($V_{mc} = V_{mf}$ in Fig. 3d) without major tectonic change (Dubille and Lavé, 2015; Schlunegger and Norton, 2015). The migration rate of the transition contains the lateral propagation and crustal shortening rates of the orogenic wedge (Fig. 3d; DeCelles and DeCelles, 2001). Therefore, it represents the sum of the lateral propagation rate of northern Tian Shan (V_p in Fig. 3d) and the absorbed crustal shortening rate (V_s in Fig. 3d). In the front of northern Tian Shan, shortening rates derived from local structure analyses are of a wide range (e.g., Avouac et al., 1993; Qiu et al., 2019), and are different from the migration rate of the transition. The reason for this difference is that the former cannot represent the propagation of the orogenic wedge but a local structure, the latter does the shortening rate of the orogen-foreland basin system. The GPS data observed during the past 25 years demonstrate that 3.2±1.0 mm/yr of crustal shortening is absorbed by Tian Shan along ~87°E (Wang and Shen, 2020), less than the migration rate of the transition in profile BB', ~4.03 mm/yr. The difference should be the lateral propagation rate of northern Tian Shan (V_p), 0.8±1.0 mm/yr.

At a thousand-year to hundred-thousand-year-time scale, dominant agents of sediment transportation and landscape evolution in the orogenic belt alternate between glacier erosion and fluvial erosion due to climatic oscillations (Deal and Prasicek, 2020; Mariotti et al., 2021). The widespread glaciation can drive higher rates of erosion and sediment production than fluvial erosion in a cold period (Shuster et al., 2005). In a warm period, the glacier terminus retreats a few tens kilometers upstream toward the hinterland, which decreases a sediment supply (e.g., Malatesta et al., 2018) and the slop of river longitudinal profile (Deal and Prasicek, 2020). These variations can substantially affect the median grain size, the fining rate of riverbed sediments along a longitudinal river, and change positions of GSTs (Paola et al., 1992; Rohais et al., 2012; Dingle et al., 2016). These climate oscillations can cause GSTs in the foreland basin to move back and forth. In northern Tian Shan, the glacier terminus moved toward the hinterland ~20 km relative to the position of the frontal moraine deposited in the Last Glacial Maximum (Fig. S6; Shi et al., 2006), which could cause the GST to migrate to the hinterland. Accordingly, we propose that the deviations between the observed and predicted positions of the conglomerate-sandstone transitions along profiles AA' and BB' is caused by the climatic oscillations in northern Tian Shan. The variation of the deviations suggests six climate cycles during 23–6 Ma, and four cycles during 3.1–0.7 Ma in northern Tian Shan (Fig. 4). The average cycle became shorter since the Pliocene, which is consistent with a change from a stable climate to one with frequent, high-amplitude variations since the Quaternary based on the deep-sea benthic foraminifer ^{13}C and ^{18}O records (Zachos et al., 2001; Westerhold et al., 2020).

A tectonic pulse could also cause backstepping of GSTs by increasing subsidence in the foreland basin paired with channel steepening of the erosional hinterland (Whipple et al., 2004), which has been detected in the Molasse basin with a low lithospheric elastic thickness of 7~15 km and a short wavelength of deflection across the basin (Schlunegger and Norton, 2015). However, the constant migration rate of the GSTs (Fig. 3) and low-temperature thermochronology do not reveal any dramatic tectonic pulse in northern Tian Shan to cause backstepping of the depocenter of the southern Junggar foreland basin (Charreau et al., 2011) with a high lithospheric elastic thickness ~50 km (Jiang, 2014).

The cycles of the deviations of the conglomerate-sandstone imaged by seismic profiles and the cycles of the erosion rates in northern Tian Shan share the same frequency over the last 10 Myr, but there is a lag time of 0.2–0.4 Myr between

them (Charreau et al., 2011; Fig.4). It may reflect the lag of gravel from the bedrock source to the foreland basin sink (Allen and Heller, 2012).

CONCLUSION

The two seismic profiles across the southern Junggar foreland basin show that the conglomerate-sandstone transitions in the basin-fill migrates forelandward at ~0.36 mm/yr along 84°E during 23–6 Ma, and migrated at ~4.03 mm/yr along 87°E during 3.1–0.7 Ma. The deviations between the observed and predicted positions of the transitions suggest six cycles of climatic oscillations during 23–6 Ma and four cycles during 3.1–0.7 Ma in northern Tian Shan area.

ACKNOWLEDGEMENTS

This work was supported by the National Natural Science Foundation of China [grant number 41672198 and 42072153] and the Fundamental Research Funds for the Central Universities [grant number B200201025]. This study benefited from discussions with Dr. Yanjun Wang, Profs. Shaowen Liu and Jinbao Su.

REFERENCES

Allen, A.P., and Heller, L.P., 2012. Dispersal and preservation of tectonically generated alluvial gravels in sedimentary basins. Tectonics of Sedimentary Basins, In: Cathy Busby and Antonio Azor. (Eds.), Tectonics of Sedimentary Basins: Recent Advances. Blackwell Publishing Ltd, pp. 111–130.

Avouac, J. P., Tapponnier, P., Bai, M., You, H., Wang, G., 1993. Active thrusting and folding along the northern Tien Shan and late Cenozoic rotation of the Tarim relative to Dzungaria and Kazakhstan. Journal of Geophysical Research: Solid Earth, 98, 6755–6804. http://dx.doi.org/10.1029/92JB01963

BGMRX (Bureau of Geological and Mineral Resources of the Xinjiang Uygur Autonomous Region), 1993. Regional geology of Xinjiang Uygur Autonomous region, People's Republic of China Ministry of Geology and Mineral Resources. Geol. Mem., 32, 841.

Burbank, D.W., Beck, R.A., Raynolds, H., Hobbs, R., Tahirkheli, K., 1988. Thrusting and gravel progradation in foreland basins - a test of post-thrusting gravel dispersal. Geology, 16, 1143–1146. http://dx.doi.org/10.1130/0091-7613(1988)0162.3.CO;2

Charreau, J., Gumiaux, C., Avouac. J.P., Augier, R., Chen, Y., Barrier, L., Gilder, S., Dominguez, S., Charles, N., Wang, Q.C., 2009a. The Neogene Xiyu Formation, a diachronous prograding gravel wedge at front of the Tianshan: Climatic and tectonic implications. Earth and Planetary Science Letters, 287, 298–310. http://dx.doi.org/10.1016/j.epsl.2012.05.033

Charreau, J., Chen, Y., Gumiaux, C., Gilder, S., Barrier, L., Dominguez, S., Augier, R., Sen, S., Avouac, J.-P., Gallaud, A., Graveleau, F., Wang, Q., 2009b. Neogene uplift of the Tian Shan Mountains observed in the magnetic record of the Jingou River section (northwest China). Tectonics, 28, TC2008. http://dx.doi.org/10.1029/2007TC002137

Charreau, J., Blard, P-H., Puchol, N., Avouac, J-P., Augier, Lallier-Verges, E., Bourles, D., Braucher, R., Gallaud, A., Finkel, R., Jolivet, M., Chen, Y., Roy, P., 2011. Paleo-erosion rates in Central Asia since 9 Ma: A transient increase at the onset of Quaternary glaciations?. Earth and Planetary Science Letters, 304, 85–92. http://dx.doi.org/10.1016/j.epsl.2011.01.018

Davis, D., Suppe, J., Dahlen, A.F., 1983. Mechanics of fold-and-thrust belts and accretionary wedges. Journal of Geophysical Research, 88, 1153-1172. http://dx.doi.org/10.1029/JB088iB02p01153

Deal, E., Prasicek, G., 2020. The Sliding Ice Incision Model: A new approach to understanding glacial landscape evolution. Geophysical Research Letters, 48, e2020GL089263. https://doi.org/10.1029/2020GL089263

DeCelles, P.G., & DeCelles, P.C., 2001. Rates of shortening, propagation, underthrusting, and flexural wave migration in continental orogenic systems. Geology, 29(2), 135-138. http://dx.doi.org/10.1130/0091-7613(2001)0292.0.CO;2

Dingle, E.H., Sinclair, H.D., Attal, M., Milodowski, D.T., and Singh, V., 2016, Subsidence control on river morphology and grain size in the Ganga Plain: American Journal of Science, 316, 778–812. https://doi .org/10.2475/08.2016.03.

Dubille, M., and Lavé, J., 2015. Rapid grain size coarsening at sandstone/conglomerate transition: similar expression in Himalayan modern rivers and Pliocene molasse deposits. Basin research, 27, 26-42. https://doi .org/10.1111/bre.12071

Duller, R.A., Whittaker, A.C., Fedele, J.J., Whitchurch, A.L., Springett, J., Smithells, R., Fordyce, S., and Allen, P.A., 2010. From grain size to tectonics. Journal Geophysical Research-Earth Surface, 115, F03022. http://dx.doi.org/10.1029/ 2009JF000409.

Fang, X., Shi, Z., Yang, S., Yan, MD, Li, J., & Jiang, P., 2002. Loess in the Tian Shan and its implications for the development of the Gurbantunggut desert and drying of northern Xinjiang. Chinese Science Bulletin, 16, 1381-1387. http://dx.doi.org/10.1360/02tb9305

Ferguson, R., Hoey, T., Wathen, S., and Werritty, A., 1996. Field evidence for rapid downstream fining of river gravels through selective transport. Geology, 24, 179–182. http://dx.doi.org/10.1130/0091-7613(1996)0242.3.CO;2

He, D., Suppe, J., Geng, Y., Shuwei, G., Shaoying, H., Xin, S., Xiaobo, W., Chaojun, Z., 2005. Guide book for field trip in south and north Tianshan foreland basin, Xinjiang Uygur Autonomous Region, China. International conference on theory and application of fault-related folding in foreland basins 77.

Jiang, X. D., 2014. Dynamic support of the Tien Shan lithosphere based on flexural and rheological modelling. Journal of Asian Earth Sciences, 93, 37-48. https://doi.org/10.1016/j.jseaes.2014.07.006

Lu, H.H., Burbank, W.D., Li, Y.L., Liu, Y.M., 2010. Late Cenozoic structural and stratigraphic evolution of the northern Chinese Tian Shan foreland. Basin Research, 22, 249-269. https://doi.org/10.1111/j.1365-2117.2009.00412.x

Malatesta, C.L., Avouac, J-P., Brown, D.N., Breitenbach, F.S., Pan, J.W., Chevalier, M-L., Rhodes, E., Saint-Carlier, D., Zhang, W.J., Charreau, J., Lave, J., & Blard, P-H., 2018. Lag andmixing during sediment transfer across the Tian Shan piedmont caused by climate-driven aggradation–incision cycles. Basin Research, 30, 613–635. https://doi.org/10.1111/bre.12267

Mariotti, A., Blard, P., Charreau, J., Toucanne, S., Jorry, J.S., Molliex, S., Bourlès, L.D., Aumaître, G., and Keddadouche, K., 2021. Nonlinear forcing of climate on mountain denudation during glaciations. Nature Geoscience, 14, 16–22. https://doi.org/10.1038/s41561-020-00672-2

Naylor, M., & Sinclair, H. D., 2008. Pro-vs. Retro-foreland basins. Basin Research, 20, 285–303. https://doi.org/10.1111/j.1365-2117.2008.00366.x

Paola, C., Heller, P.L., Angevine, C.L., 1992. The large-scale dynamics of grain-size variation in alluvial basins, 1: Theory. Basin Research, 4(2), 73–90. https://doi.org/10.1111/j.1365-2117.1992.tb00145.x

Qiu, J.H., Rao, G., Wang, X., Yang, D.S., Xiao, L.X., 2019. Effects of fault slip distribution on the geometry and kinematics of the southern Junggar fold-and-thrust belt, northern Tian Shan. Tectonophysics, 772, 228209. https://doi.org/10.1016/j.tecto.2019.228209

Rohais, S., Bonnet, S., Eschard, R., 2012. Sedimentary record of tectonic and climatic erosional perturbations in an experimental coupled catchment-fan system. Basin Research, 24, 198–212. https://doi.org/10.1111/j.1365-2117.2011.00520.x

Schlunegger, F., Norton, K., 2015. Climate vs. tectonics: the competing roles of Late Oligocene warming and Alpine orogenesis in constructing alluvial megafan sequences in the North Alpine foreland basin, Basin Research, 27, 230–245. https://doi.org/10.1111/bre.12070

Shi, Y.F., Cui, Z.J., Su, Z., 2006. The Quaternary Glaciations and Environmental Variations in China. Hebei, Science and Technology Press, 1–618．(in Chinese)

Shuster, D.L., Ehlers, T.A., Rusmore, M.E., Farley, K.A., 2005. Rapid glacial erosion at 1.8 Ma revealed by $^{4}He/^{3}He$ thermochronometry. Science 310, 1668–1670. https://doi.org/10.1126/science.1118519

Wang, M., & Shen, Z.-K., 2020. Present-day crustal deformation of continental China derived from GPS and its tectonic implications. Journal of Geophysical Research: Solid Earth, 125, e2019JB018774. https://doi.org/10.1029/2019JB018774

Wang, S.L., Chen, Y., Charreau, J., Li, Y.X., Chen, Z.X., Zhu, G.Y., Xu, H.Z., Li, C., and Wang, L.S., 2021. Underthrusting of the Tarim lithosphere beneath the western Kunlun range, insights from seismic profiling evidence. Tectonics, 40, e2019TC005932. https://doi.org/10.1029/2019TC005932

Westerhold, T., Marwan, N., Drury, J.A., Liebrand, D., Agnini, C., Anagnostou, E., Barnet, S.J., Bohaty, M.S., Vleeschouwer, D.D., Florindo, F., Frederichs, T., Hodell, A.D., Holbourn, E.A., Kroon, D., Lauretano, V., Littler, K., Lourens, J.L., Lyle, M., Pälike, H., Röhl, U., Tian, J., Wilkens, H.R., Wilson, A.P., and Zachos, C.J., 2020. An astronomically dated record of Earth's climate and its predictability over the last 66 million years. Science, 369 (6509), 1383–1387. https:// doi.org/10.1126/science.aba6853

Whipple, K.X., 2004. Bedrock rivers and the geomorphology of active orogens. Annual Review of Earth and Planetary Sciences, 32, 151–185. https://doi.org/10.1146/annurev.earth.32.101802.120356.

Whittaker, C.A., Duller, R.A., Springett, J., Smithells, A.R., Whitchurch, L.A., Allen, A.P., 2011. Decoding downstream trends in stratigraphic grain size as a function of tectonic subsidence and sediment supply. Geological Society of America Bulletin, 123(7/8), 1363–1382. http://dx.doi.org/10.1130/B30351.1

Windley, B.F., Allen, M.B., Zhang, C., Zhao, Z.Y., Wang, G.R., 1990. Paleozoic accretion and Cenozoic deformation of the Chinese Tien Shan Range, central Asia. Geology 18, 128–131. https://doi.org/10.1130/0091-7613(1990)018<0128:PAACRO>2.3.CO;2

Zachos, J., Pagani, M., Sloan, L, Thomas, E., Billups, K., 2001, Trends, Rhythms, and Aberrations in Global Climate 65 Ma to Present, V. 292(5517), 686-693. http://dx.doi.org/10.1126/science.1059412

Zhang, P., Molnar, P., Downs, W.R., 2001. Increased sedimentation rates and grain sizes 2–4 Myr ago due to the influence of climate change on erosion rates. Nature 410, 891–897. http://dx.doi.org/10.1038/35073504

Zhou, M.L., 1988. China Quaternary System, Stratigraphy of China (14). Beijing Geological Publishing House, 1-276. (in Chinese)

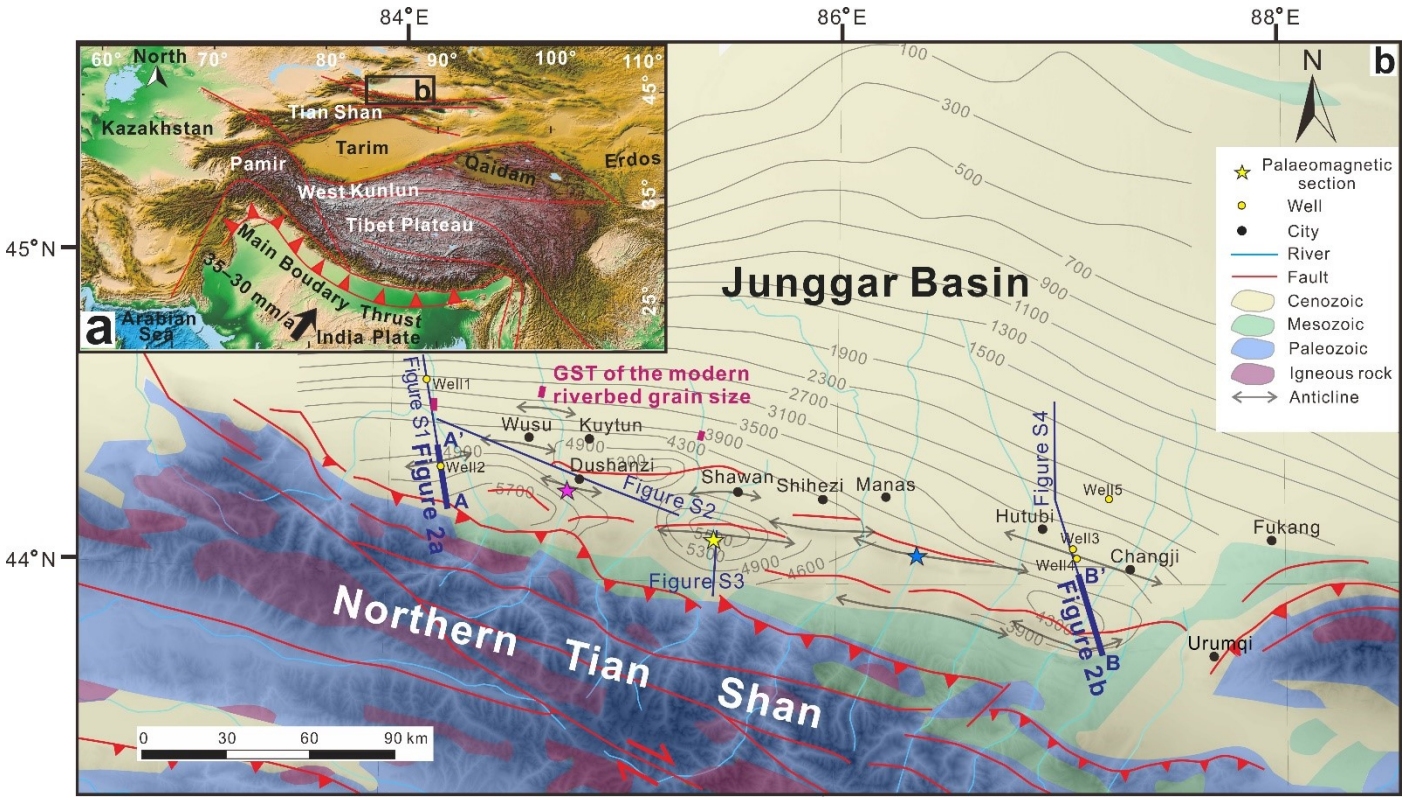

Fig. 1. (a) Location of the modern Tian Shan intracontinental orogen within the India-Tibet collision system. **(b)** Geological sketch and thickness contours (unit: m) of the Cenozoic successions in the southern Junggar foreland basin (BGMRX, 1993). Locations of Figs. 2a, 2b are marked by the dark blue thick lines, and locations of Figs. S1, S2, S3 and S4 are marked by the dark blue thin lines. Yellow dots represent drill holes. Stars mark the magnetostratigraphic sections.

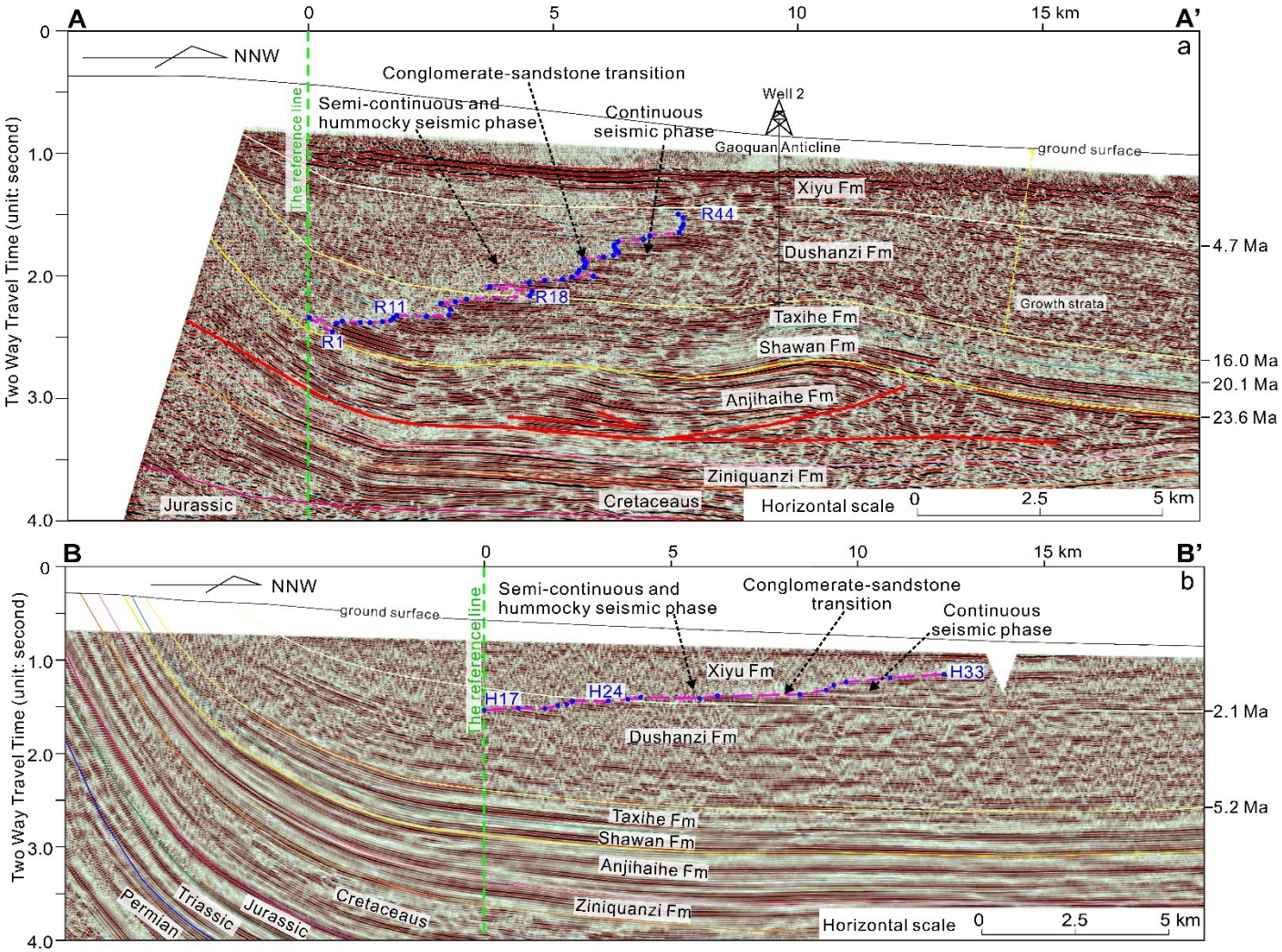

Fig. 2. Interpreted seismic profile AA' **(a)** and BB' **(b)** across the southern Junggar foreland basin. See Fig. 1b for locations. The purple dashed lines indicate the traces of the conglomerate-sandstone transitions in deposit layers of the basin-fill. The green vertical lines are the reference line in the profiles. The formations' boundaries in the seismic profile are determined based on well logging, outcrop data near the profiles, and previous interpretations of seismic profiles in the basin (e.g. Qiu et al., 2019).

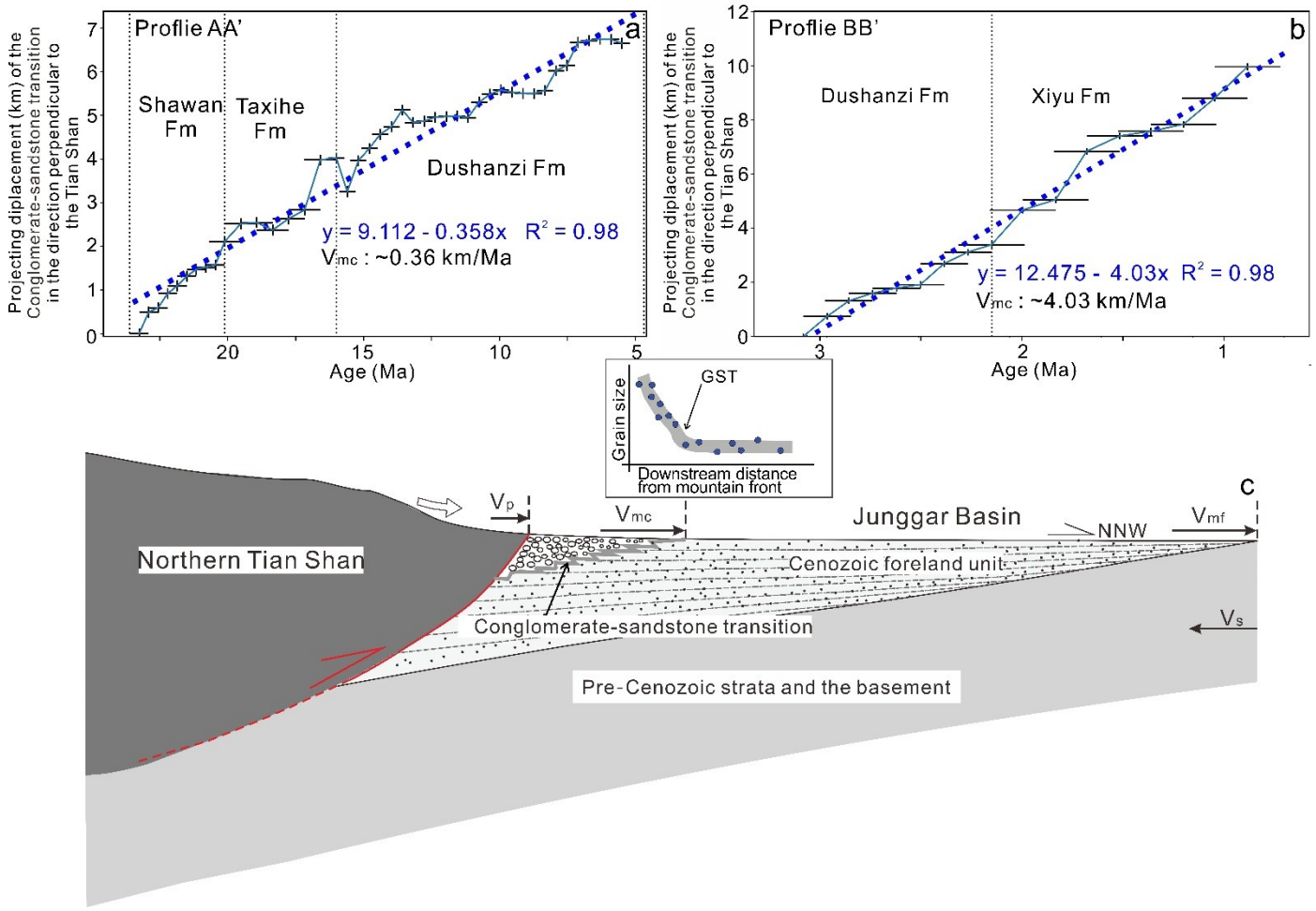

Fig. 3. The linear regression models of the positions and ages of the conglomerate-sandstone transitions in profile AA' **(a)** and BB' **(b)**. Observed positions of the transitions are indicated by the light blue solid lines, and the deep blue dashed lines marked the fitted lines. **(c)** Schematic sketch of the relationship of the migration rates of the conglomerate-sandstone transition (V_{mc}) and the foreland basin (V_{mf}), the rate of lateral propagation of the orogenic wedge (V_p) and the crustal shortening rate (V_s) in the orogen-foreland basin system.

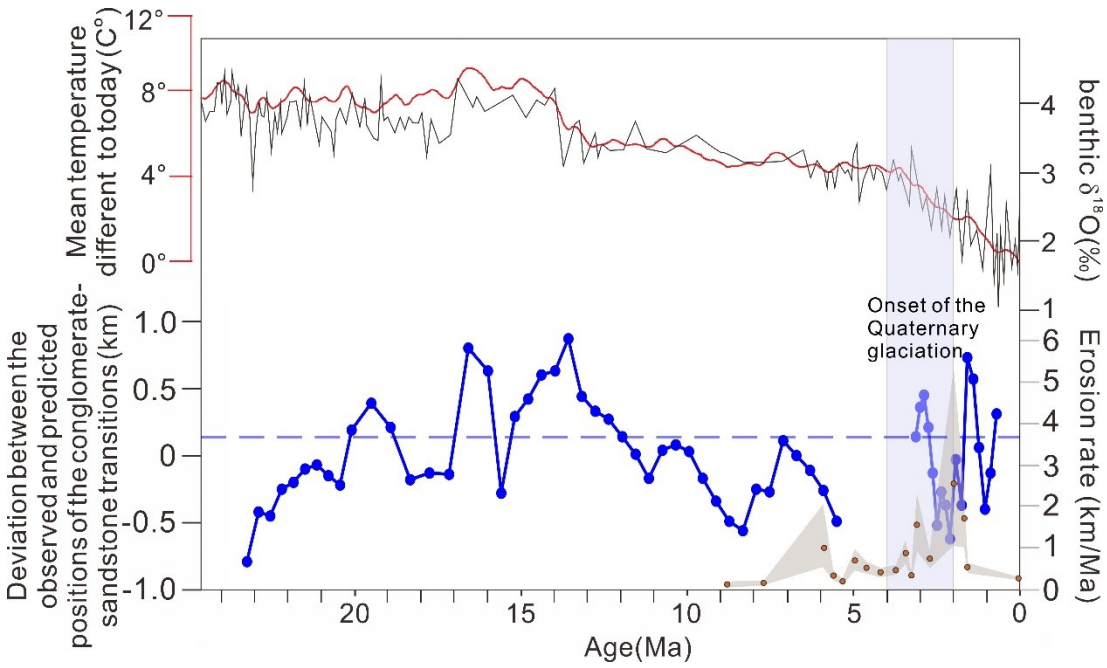

Fig. 4. Deviations between the observed and predicted positions of the conglomerate-sandstone transitions in the basin infill of the southern Junggar foreland basin (dark blue solid lines), erosion rates in the hinterland area of the orogen (gray shadow) (Charreau et al., 2011) and global deep-sea oxygen isotope record (black and red solid lines) (Zachos et al., 2001; Westerhold et al., 2020) since 25 Ma.